Statistical Evaluation of the Coupling Effects between Tags in a UHF RFID Forward Link

Aiman Mughal, Jithin Mudakkarappilli Sudersanan, Shermila Mostarshedi, Benoit Poussot, Jean-Marc Laheurte

Statistical Evaluation of the Coupling Effects between Tags in a UHF RFID Forward Link

Aiman Mughal, Jithin Mudakkarappilli Sudersanan, Shermila Mostarshedi, Benoit Poussot, Jean-Marc Laheurte

***Abstract*—The aim of this paper is to propose a statistical analysis of the performance of an RFID system in a high-density context, based on a physical model which takes into account the mutual coupling and random position of tags. The read-range of an isolated tag is measured and validated from simulation. The degradation in terms of read-range and the power absorbed by the RFID chip is analysed in the presence of surrounded short-circuited tags. Then a set of randomly distributed RFID tags are modelled by a set of loaded half-wave dipoles distributed over an electrically small area to observe the absorbed power on circuit-level. An impedance matching technique employing a T-match has been adapted with dipoles for maximum power transfer in the forward link. The coupling effects taking into account the randomness of dipoles are studied using linear and circular polarisations of the incident field. Numerical Electromagnetics Code (NEC) simulator and High-Frequency Structure Simulator (HFSS) are used for the assessment of forward links for dipoles (with and without T-match) and tags respectively.**

***Index Terms*—RFID system, coupled tags, read-range, T-match, statistical analysis**

I. Introduction

THE radio-frequency identification (RFID) technology plays a well-established role in the tracking and identification of objects. Many a time, it is utilised in a high-density context in applications such as industrial laundry, real-time tracking of livestock, cargo and supply-chain logistics, and other similar scenarios where the concentration of RFID tags is high, and they are stacked in a reduced volume [1]. In such a frame of reference, there would be a strong electromagnetic coupling among the tags and with the surroundings, which could degrade the communication link between the reader and the tag. Furthermore, as the position and orientation of tags in a high-density context are often arbitrary, the matching and radiation properties of a tag would experience random variations, which differ from one configuration to another. Various techniques such as using multiple readers, using low scattering antennas [2], introducing load switching at the neighboring antennas [3], or stirring the surrounding environment of the tags [4] can be employed to deal with these practical constraints. The readability of RFID tags has been analysed in the literature using various experimental approaches, followed by statistical analysis of the empirical data using regression models or other advanced techniques. The statistical analysis can be based on variability of the performance metrics of one tag [5], [6] or multiple tags [7], [8] versus the surrounding environment.

The authors are affiliated with Univ Gustave Eiffel, CNRS, ESYCOM, F-77454 Marne-la-Vallée, France (email: aiman.mughal@univ-eiffel.fr)

This paper aims to analyse and quantify the degradation in the RFID communication link in a high-density context. To our knowledge, statistical analysis has not been applied before in the physical layer of an RFID link, notably to assess the electromagnetic phenomenon of coupling. As the study focuses primarily on the forward link and the associated absorbed power to wake up the tag, we estimated the percentage of active tags involved in the evaluation of the link budget between the RFID reader with a given transmitted power, and a set of randomly distributed tags located at a given distance. The electromagnetic field introduced by the reader can be chosen to be linearly or circularly polarised. An investigation of the similarity between tags and half-wave dipoles is also performed in terms of power absorbed by the load. It is important to note that their intrinsic properties would be different, and hence statistically generated cumulative distribution function (CDF) plots could be used to establish a correlation between their behaviours.

The manuscript is an extended version of [9] and is organised as follows: in Section II, a proof of concept is presented. The degradation of the read-range, as an output of an RFID communication link, is investigated as the responding tag is exposed to coupling effects. In Section III, an RFID system consisting of a set of N randomly distributed tags over an electrically small area is modelled by a set of dipoles, followed by the network representation of the forward link of RFID communication. Section IV presents the distribution of power at various levels of the antenna based on the network model, for isolated cases and a chosen random distribution. The statistics of absorbed power in the forward link of RFID communication for the set of dipoles, tags, and dipoles with a matching network are presented in Section V.

II. RFID performance exposed to coupling effects

In this section, the read-range of a real RFID link is studied, when it is exposed to the coupling effects between tags. In order to quantify the degradation of the read-range with respect to the coupling level, a home-made RFID tag is used. The read-range of a single tag is compared to that of the same tag when surrounded by other short-circuited tags. Short-circuit is chosen for the sake of simplicity of the realisation and also to increase the coupling effects. To this aim, the selected RFID chip and the designed antenna need to be characterised. The characterisation involves the measurement of the impedance of both the antenna and the chip using different power levels to include non-linearities in chip impedance.

During this procedure, three pieces of equipment are used: the Voyantic Tagformance system to determine the power

sensitivity of the chip, the Keysight technologies E4991B impedance analyzer used along with the 16194A component test fixture to measure the complex chip impedance, and the ZNB 8 Vector Network Analyser (VNA) to measure the complex input impedance of the tag antenna. Proper calibrations are performed on the impedance analyser and the VNA, over the frequency band of 850 MHz–990 MHz. For measuring chip sensitivity, a standard 50 Ω SMA connector is soldered to the chip and connected to the Voyantic system to measure the minimum input power level $P_{T_{\text{th}}}$ necessary to activate the chip. Then, the chip is placed between the two electrodes of the impedance analyser whose input power is set to $P_{T_{\text{th}}}$. The measured Z_{L} is the chip impedance at the threshold power level. Furthermore, the complex input impedance of the home-made tag antenna is measured with a VNA using a differential excitation technique explained in [10].

A. *Characterisation of the tag antenna and the chip*

For the sake of simplicity of measurement, we chose the encapsulated Alien "Higgs-9" RFID chip [11] enclosed in a SOT323 package, as the experimental chip for our proof of concept, as it can be easily measured and soldered to the tag antenna. We designed a capacitively loaded meandered dipole antenna which is conjugately matched to the chip at 862 MHz. A schematic of the designed tag antenna with its dimensions is shown in Fig. 1. The design of this tag antenna is based on that of a real commercial UHF RFID tag manufactured by Alien Technology (ALN-9662), etched on a plastic substrate, which will be used later in this study. The home-made tag has been realised on an FR4 substrate. The properties of the substrate have been adjusted through reverse simulations with respect to the measurements.

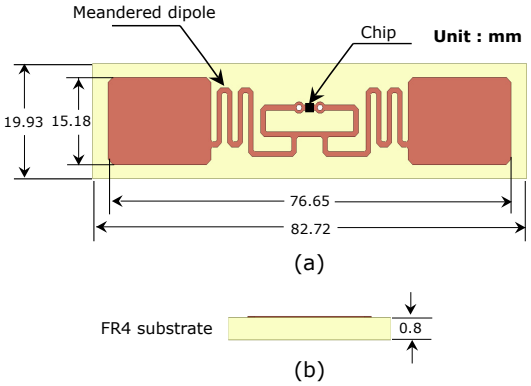

Fig. 1: Schematic of the home-made RFID tag with its dimensions (top view in (a) and side view in (b)).

The complex input impedance of an isolated tag antenna is simulated by HFSS and measured using the procedure explained earlier by a differential probe in an anechoic chamber. The chip impedance varies with the input power and hence, the minimum input power as measured from Voyantic cabinet ($P_{T_{\text{th}}} = P_{T_2} = -9.2$ dBm) was utilised to measure the input impedance using the impedance analyser. The antenna and the chip impedances measured at P_{T_2} (red solid line) and two other power values around P_{T_2} are shown in Fig. 2.

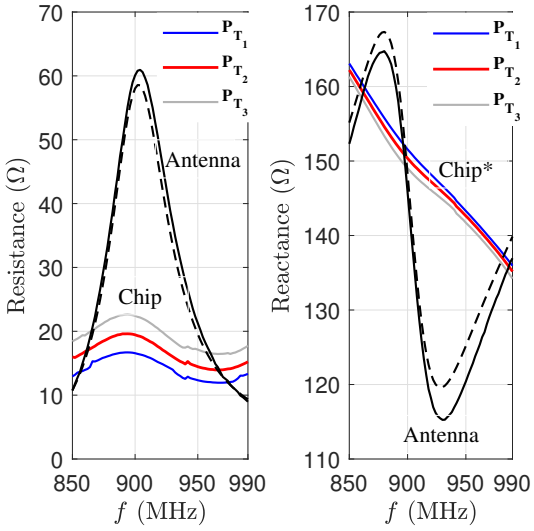

Fig. 2: Simulated (black dashed line) and measured (black solid line) impedance of the home-made tag antenna of Fig. 1 along with measured chip impedance (Higgs-9) for different measured input powers $P_{T_1} = -9.6$ dBm, $P_{T_2} = -9.2$ dBm, and $P_{T_3} = -8.8$ dBm.

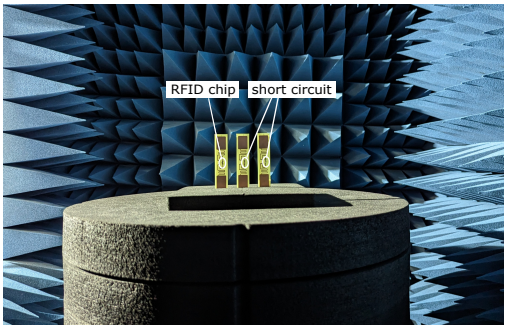

Fig. 3: Three parallel tags placed inside the Voyantic cabinet for read-range measurements.

B. *Read-range analysis*

The tag antenna connected to its chip is further used to estimate the read-range in different configurations using the Voyantic cabinet (Fig. 3). The maximum reading range is related to the power absorbed by the chip using the following equation [12]:

$$d_{\text{max}} = \sqrt{\frac{P_{\text{EIRP}_{\text{max}}} G_{\text{tag}} (1 - |\Gamma|^2)}{P_{L_{\text{th}}}}} \frac{\lambda}{4\pi} \tag{1}$$

where, $P_{\text{EIRP}_{\text{max}}}$ is the maximum regulated effective isotropic power radiated by the reader antenna, $P_{L_{\text{th}}}$ is the chip sensitivity, G_{tag} is the gain of the tag antenna, and $|\Gamma|$ is the reflection coefficient due to the mismatch between the tag antenna and chip, expressed as:

$$|\Gamma| = \left| \frac{Z_{\text{L}} - Z_{\text{a}}^*}{Z_{\text{L}} + Z_{\text{a}}} \right| \tag{2}$$

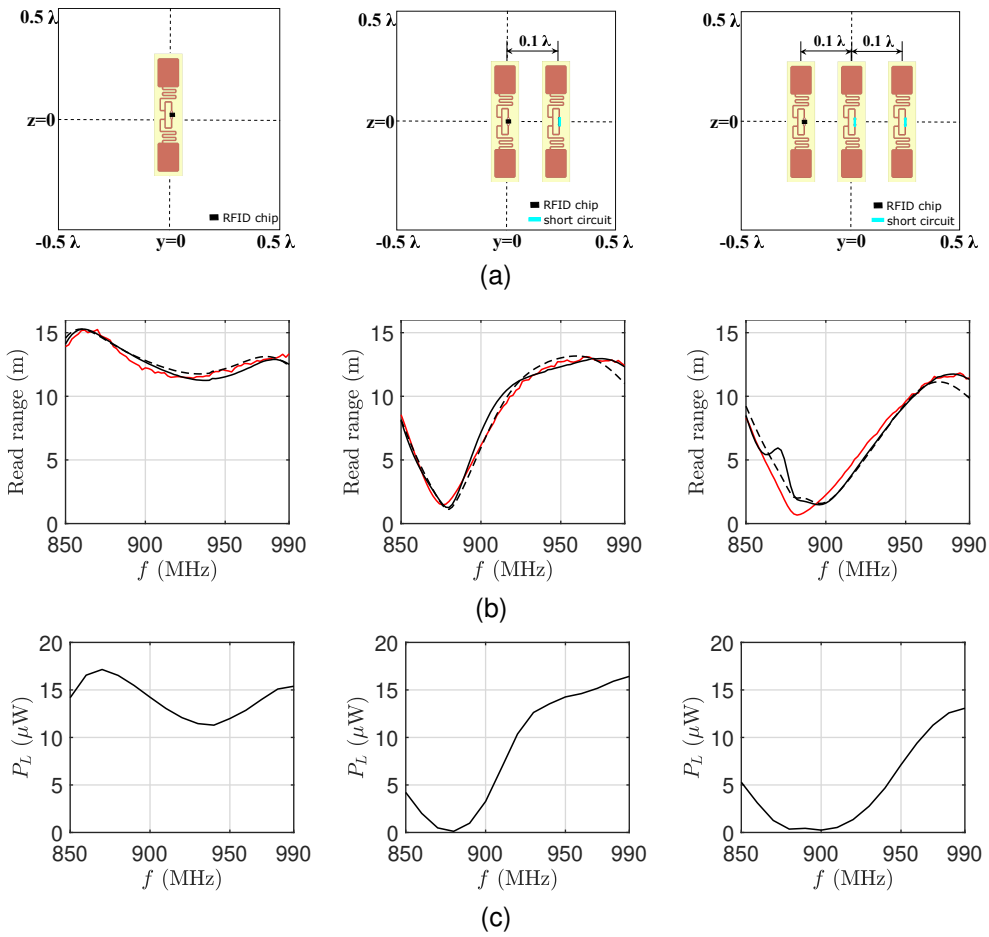

Fig. 4: Three configurations of tags shown in (a), with the read-range [measured (red solid line), estimated from measured Z_{a} (black solid line) and from simulated Z_{a} (black dashed line)] in (b), and absorbed power (P_L) estimated using HFSS in (c).

where Z_{L} is the chip impedance and Z_{a} is the impedance of the tag antenna of interest.

In this study the $P_{\mathrm{EIRP_{max}}}$ is fixed to 3.28 W, G_{tag} is obtained from HFSS, and $|\Gamma|$ is calculated using impedances presented in Fig. 2. The sensitivity of the chip $P_{L_{\mathrm{th}}}$ is obtained from Voyantic measurement as explained in [13] by $P_{L_{\mathrm{th}}} = P_{T_{\mathrm{th}}}(1 - |\Gamma_{50\Omega}|^2)$. The estimated read-range can thus be compared to the read-range measured from Voyantic. Three configurations are studied to observe the degradation in the read-range of an isolated tag antenna in the presence of other short-circuited tags. Figure 4(a) shows an isolated tag as well as two configurations including two and three parallel tags, placed at a given distance from each other. The measured and estimated read-ranges are presented in Fig. 4(b). A decent agreement is observed among the three techniques which validates our experimental setup. For the rest of the study, we would like to replace the read-range which is a system-level observable by the power absorbed by the chip which is a circuit-level output. The absorbed power at the chip level can be estimated using HFSS as:

$$P_L = \frac{1}{2}\Re\left(V_L I_L^*\right) = \frac{1}{2}\left|\frac{V_{\mathrm{L}}}{Z_L}\right|^2 \Re(Z_L) \qquad (3)$$

where V_{L} is the induced voltage at the level of the chip when the tag is illuminated with a plane wave (E = 1 V/m). The absorbed power (P_{L}) is plotted in Fig. 4(c) for different tag configurations. The evolution of P_{L} over the frequency band is consistent with that of the read-range, which shows that the power absorbed by the chip is a good candidate to analyse the performance of the RFID link exposed to coupling effects. Further, we can add more complexities to the configurations by presenting a simplified model for the tag.

III. Modelling of the RFID forward link

Fig. 5(a) presents a classic network model of an RFID system consisting of a random distribution of N tags over a specific area in the yoz plane, illuminated by a reader positioned at a point in space (here on the x-axis). The tag centers are assumed to be randomly distributed such that they do not overlap.

In the forward link, the reader transmits continuous wave (CW) signals and modulated commands to the tag. The tag harvests energy from the incident electromagnetic field to energise the communication and processing circuits, and consequently feed the chip. In the backward link, the tag responds by switching its chip impedance between two distinct

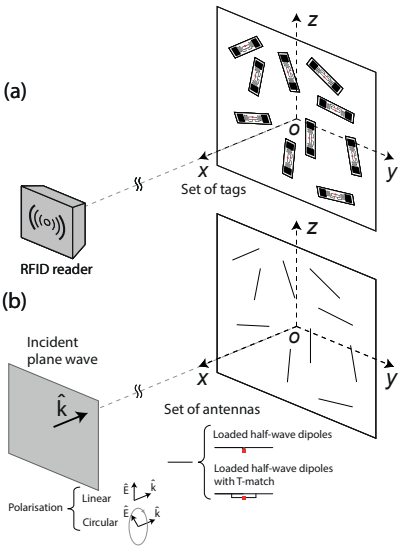

Fig. 5: Set of RFID tags and the reader in (a) modelled by loaded dipoles illuminated by a plane wave in (b).

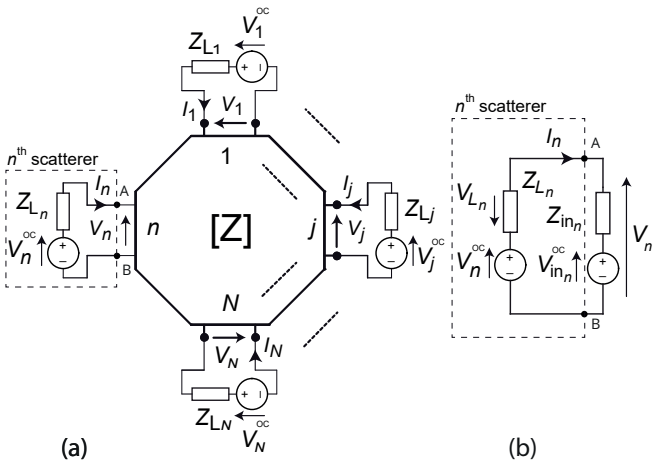

Fig. 6: Equivalent circuit model of (a) N loaded dipoles exposed to an incident electromagnetic wave (b) the circuit as seen by the n^{th} dipole.

states, thereby modulating the signal backscattered to the reader, containing the information stored in its data memory. In the context of high-density tagged objects, both links are subject to degradation, among other reasons, as a result of the electromagnetic coupling between tags.

In this work, we focus to analyse the quality of the forward link taking into account, the polarisation of the reader, the random position, and the orientation of the tags. In order to reduce the complexity of the scenario, a simplified model is presented in Fig. 5(b). The reader illuminating the set of scatterers is assumed to be an incident plane wave, linearly or circularly polarised. On account of the statistical similarities discussed in [14], the tag antennas are modelled by half-wave dipoles, including a T-match network or not. The dipoles representing the tags are loaded. The centers and orientations of the N dipoles are supposed to be the same as that of the randomly distributed tags. The study will cover both deterministic and statistical approaches in terms of the power received at various levels of the tag. The chip sensitivity, which is defined as the minimum turn-on power, will be utilised to draw inferences on the percentage of tags which would be activated and take part in the communication.

As introduced in [15] and [16], a set of loaded scatterers illuminated by an electromagnetic field can be modelled by an equivalent circuit model shown in Fig. 6(a). The electromagnetic field is accounted for by a series of open-circuit voltages included in the vector $[\mathbf{V}_{\text{OC}}]$, the "load network" contains N terminating load impedances represented by the vector $[\mathbf{Z_L}]$, and the "scatterer network" takes into account all couplings and is introduced by the $N \times N$ impedance matrix $[\mathbf{Z}]$.

For the forward link analysis, the circuit between A and B nodes as seen by the n^{th} dipole can be replaced by a Thevenin equivalent model as shown in Fig. 6(b). The Thevenin model is composed of an overall open-circuit voltage $V_{\text{in}_n}^{\text{OC}}$ which accounts for all V^{OC} sources on the remaining $N-1$ ports and the input impedance Z_{in_n} of the overall network as seen by the n^{th} driven dipole, which includes all couplings. The voltage across the load of the driven dipole can be computed as follows:

$$V_{L_n} = \frac{Z_{L_n}}{Z_{\text{in}_n} + Z_{L_n}} \left(V_n^{\text{OC}} - V_{\text{in}_n}^{\text{OC}}\right) \tag{4}$$

where Z_{in_n} can be computed using the modified impedance matrix of the network shown in Fig. 6(a) by the following equation [14]:

$$Z_{\text{in}_n} = \frac{1}{\mathbf{Z}_{\text{mod}_\mathbf{n}}^{-\mathbf{1}}(n,n)} \tag{5}$$

where the modified impedance matrix $\mathbf{Z}_{\text{mod}_\mathbf{n}}$ is obtained by adding the dipole loads over the corresponding diagonal elements of the impedance matrix $\mathbf{Z}$ except for Z_{nn}:

$$\mathbf{Z}_{\text{mod}_\mathbf{n}} = \begin{bmatrix} Z_{11}+Z_{L_1} & \cdots & Z_{1i} & \cdots & Z_{1n} & \cdots & Z_{1N} \\ \vdots & & & & & & \\ Z_{j1} & \cdots & Z_{jj}+Z_{L_j} & \cdots & Z_{jn} & \cdots & Z_{jN} \\ \vdots & & & & & & \\ Z_{n1} & \cdots & Z_{ni} & \cdots & Z_{nn} & \cdots & Z_{nN} \\ \vdots & & & & & & \\ Z_{N1} & \cdots & Z_{Ni} & \cdots & Z_{Nn} & \cdots & Z_{NN}+Z_{L_N} \end{bmatrix} \tag{6}$$

The equivalent model of Fig. 6(b) offers the possibility to draw up the power budget of the network. Two power values can be calculated at the level of the voltage sources. $P_{V_n^{\text{OC}}}$ is the power induced at the level of the n^{th} dipole by the plane wave :

$$P_{V_n^{\text{OC}}} = \frac{1}{2}\Re\left(V_n^{\text{OC}} I_n^*\right) \tag{7}$$

while $P_{V_{\text{in}_n}^{\text{OC}}}$ is the power induced by the $N-1$ dipoles at the level of the n^{th} dipole by mutual coupling effects :

$$P_{V_{\text{in}_n}^{\text{OC}}} = \frac{1}{2}\Re\left(V_{\text{in}_n}^{\text{OC}} I_n^*\right) \tag{8}$$

The algebraic sum of these two powers is divided between the two loads. The most important power for the forward link

analysis is the absorbed (collected) power of the n^{th} dipole or tag which can be calculated by:

$$P_{L_n} = \frac{1}{2}\Re\left(V_{L_n} I_n^*\right) = \frac{1}{2}\left|\frac{V_n^{\text{OC}} - V_{\text{in}_n}^{\text{OC}}}{Z_{L_n} + Z_{\text{in}_n}}\right|^2 \Re(Z_{L_n}) \quad (9)$$

The tag will be powered up if the absorbed power is greater than the minimum required power, i.e. the sensitivity of the chip. The other part of the total induced power goes to Z_{in_n} which can be considered as the power which will be re-radiated in the backward link and can be expressed by:

$$P_{\text{in}_n} = \frac{1}{2}\left|\frac{V_n^{\text{OC}} - V_{\text{in}_n}^{\text{OC}}}{Z_{L_n} + Z_{\text{in}_n}}\right|^2 \Re(Z_{\text{in}_n}) \quad (10)$$

Although this power is not of main interest in this paper, it provides a better understanding of the physical phenomenon during the analysis of the power budget.

IV. Deterministic analysis

To provide a more realistic representation and to analyse the reliability of the forward RFID link in a real case scenario, we will employ a commercial RFID tag for the simulations presented from this point. The commercial UHF RFID tag (ALN-9662) [17] used in our study is presented in Fig. 7(a). We fix the working frequency according to North American UHF RFID band at 928 MHz. The chip of the tag is connected to the antenna through a matching network, commonly called T-match. This tag is based on a printed capacitively loaded meandered dipole. The tag antenna has been modelled with Ansys HFSS EM simulator. Typically, the tag antenna has an input impedance with a low resistive part and a very high reactive part in order to match the impedance of the RFID chip. The simulation result showing the impedance of the tag antenna is presented in Fig. 8 over a frequency band. According to the equivalent circuit model of the RFID chip [18], i.e. a resistance R_p in parallel with a capacitance C_p respectively equal to 1500 Ohms and 0.85 pF, the complex conjugate of the input impedance of the chip over the frequency band is also included the figure. As expected, at the working frequency, i.e. 928 MHz, the input impedance of the tag antenna ($23.6+j197.9\ \Omega$) and the input impedance of the chip ($26.66 - j198.2\ \Omega$) are quasi complex conjugate to allow an efficient power transfer.

A full-wave 3D solver to predict the behaviour of this complex tag antenna in various configurations requires significant computer resources and would be time-consuming. To handle this issue, considering the dipole-like radiation properties of the tag according to the technical documentation, we propose to replace the tag antenna with a half-wave dipole. Consequently, the dipole can be designed with a matching network to be closer to the initial tag antenna topology following [19] and [20] as shown in Fig. 7(b), or a simpler equivalent model can be adopted using a dipole without the matching network as in Fig. 7(c). The structure of the dipole with T-match is based on the insertion of a second folded dipole connected to the center of the first dipole. The two simpler wire antennas allow the use of 4NEC2 solver, an electromagnetic simulator based on Method of Moments and is adapted to analyse structures

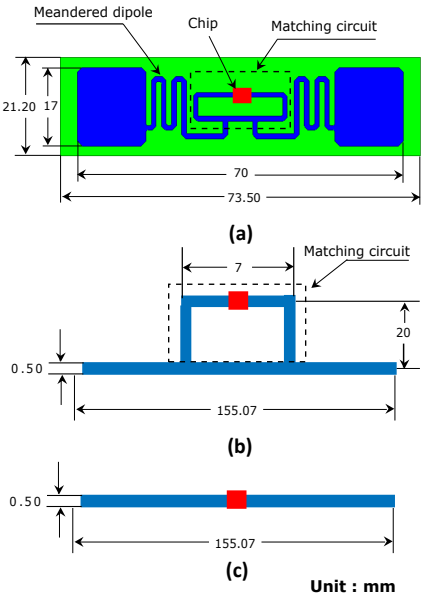

Fig. 7: Schematic of (a) tag (b) T-matched dipole and (c) dipole, indicating their respective dimensions.

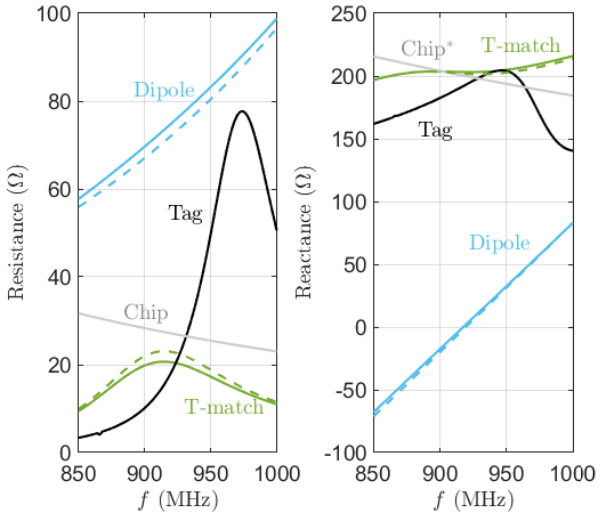

Fig. 8: Real and imaginary parts of the impedance of the commercial tag and the dipole with and without T-match using HFSS (solid line) and NEC (dashed line).

including wires and surfaces in free space or over a ground [21]. The input impedance of a dipole with and without T-match has been simulated by 4NEC2 and compared to HFSS in Fig. 8.

The comparison in Fig. 8 shows that 4NEC2 would be sufficient to estimate the impedance of the wire antennas. We will show later that this is not only true for the isolated case, but also for configurations including coupling effects. On the other hand, we observe that the impedance values for the three antennas over the frequency band are different. The impedance values at 928 MHz which are used in this study are presented in Table I.

The following parts will present both the deterministic and

TABLE I: Input impedance of the three isolated antennas at 928 MHz

	Dipole	T-match	Tag
HFSS	$77.0 + j10.5\ \Omega$	$20.0 + j203.2\ \Omega$	$23.6 + j197.9\ \Omega$
NEC	$74.2 + j8.7\ \Omega$	$22.2 + j201.5\ \Omega$	—

statistical analysis of the forward link in terms of the power by using the equivalent circuit model presented in Section III. The idea is to show that the dipole would be a good candidate to model the behaviour of the tag in the forward link. The amount of power at the level of the driven element of interest is a function of both its tilt with regard to the incident wave polarisation and the coupling with the surrounding elements. So, it would be interesting to refer to the power at various circuit levels of an isolated element, as it would represent an ideal communication scenario from the reader to the tag, due to the absence of any coupling effects.

A. Isolated case

An isolated half-wave dipole, T-matched dipole, and tag are placed symmetrically about the origin along the z-axis as shown in Fig. 9. 4NEC2 is used to simulate the half-wave dipole, with and without T-match, while the tag is simulated with Ansys HFSS. The power at various circuit levels of the isolated element employing linear and circular polarisations of the incident field ($E_Z = 1$ V/m) are presented in Table II and Table III, respectively.

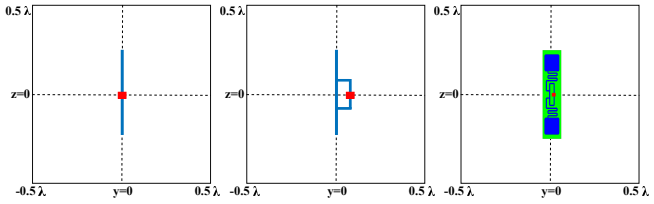

Fig. 9: Isolated (a) dipole, (b) T-matched dipole, and (c) tag, illuminated by a plane wave.

TABLE II: Isolated power for Linear Polarisation (LP)

	Dipole		T-match		Tag	
	dBm	μW	dBm	μW	dBm	μW
P_{Voc}	-14.4	36.1	-14.3	37.2	-14.8	33.1
P_{in}	-17.4	18.1	-17.3	18.6	-17.9	16.2
P_{L}	-17.4	18.1	-17.3	18.6	-18.1	15.5

TABLE III: Isolated power for Circular Polarisation (CP)

	Dipole		T-match		Tag	
	dBm	μW	dBm	μW	dBm	μW
P_{Voc}	-17.4	18.1	-17.3	18.6	-17.8	16.6
P_{in}	-20.4	9.0	-20.3	9.3	-20.8	8.3
P_{L}	-20.4	9.0	-20.3	9.3	-21.1	7.7

In all three cases, the power induced by the plane wave ($P_{V^{\text{OC}}}$) is almost equally divided between the load and the antenna impedance ($Z_{L_n} = Z_{11}^*$). P_{L} and $P_{V_{\text{in}}}$ represent respectively the power absorbed by the load (chip) and the re-radiated power. In the absence of surrounding elements, the power induced by coupling effects ($P_{V_{\text{in}}^{\text{OC}}}$) is null. Due to the polarisation mismatch between the linearly polarised antenna and the incident wave, the power values corresponding to circular polarisation are 3 dB lower than the power levels in the case of linear polarisation. The power levels are very close for the dipole with and without T-match and differ more for those of the tag.

B. Randomly distributed case

Let us consider an area of dimensions $1\lambda \times 1\lambda$ in yoz plane where ten identical half-wave matched dipoles are distributed randomly, as shown in Fig. 10. Each dipole has random center coordinates and orientation following a uniform distribution. The set of dipoles is illuminated by linearly and circularly polarised plane waves at normal incidence.

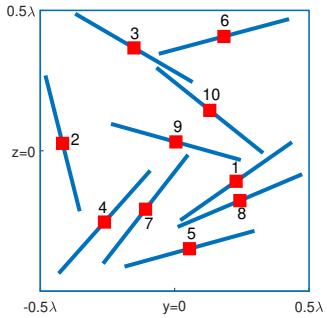

Fig. 10: Ten loaded half-wave dipoles randomly distributed over a surface of dimensions $1\lambda \times 1\lambda$.

Using 4NEC2, the open-circuit voltage (V_n^{OC}) across each loaded dipole has been obtained, while all others are open-circuited. In a second simulation, the plane wave is removed, and the dipoles are driven by their respective V_n^{OC}, while being terminated on their matched load ($Z_{L_n} = Z_{11}^*$). Consequently, the different electrical quantities in Fig. 6(b) have been calculated. Fig. 11 illustrates for each dipole, from 1 to 10, the power budget in μW for both linearly and circularly polarised plane waves.

Initially, each dipole has been considered in the absence of the others, but in its original position and orientation, i.e. the mutual coupling has been suppressed and only the orientation of the dipoles is taken into consideration. The power budget corresponding to this case is shown in the first row of Fig. 11. We observe that for the linear polarisation (LP), the power at the level of the source $P_{V_n^{\text{OC}}}$ is different for each dipole with respect to its tilt, while for the circular polarisation (CP), this power is equal, irrespective of the orientation. In the absence of coupling, the power induced by the other dipoles $P_{V_{\text{in}_n}^{\text{OC}}}$ is obviously null for both polarisations. The power induced by the plane wave is equally divided between the two loads, as is expected in the case of the matched load. In fact, without mutual coupling ($Z_{\text{in}_n} = Z_{11}$), the absorbed and the re-radiated power values are consequently identical ($P_{L_n} = P_{\text{in}_n}$).

Subsequently, all 10 dipoles are treated together. The corresponding power budget is shown in the second row of Fig. 11.

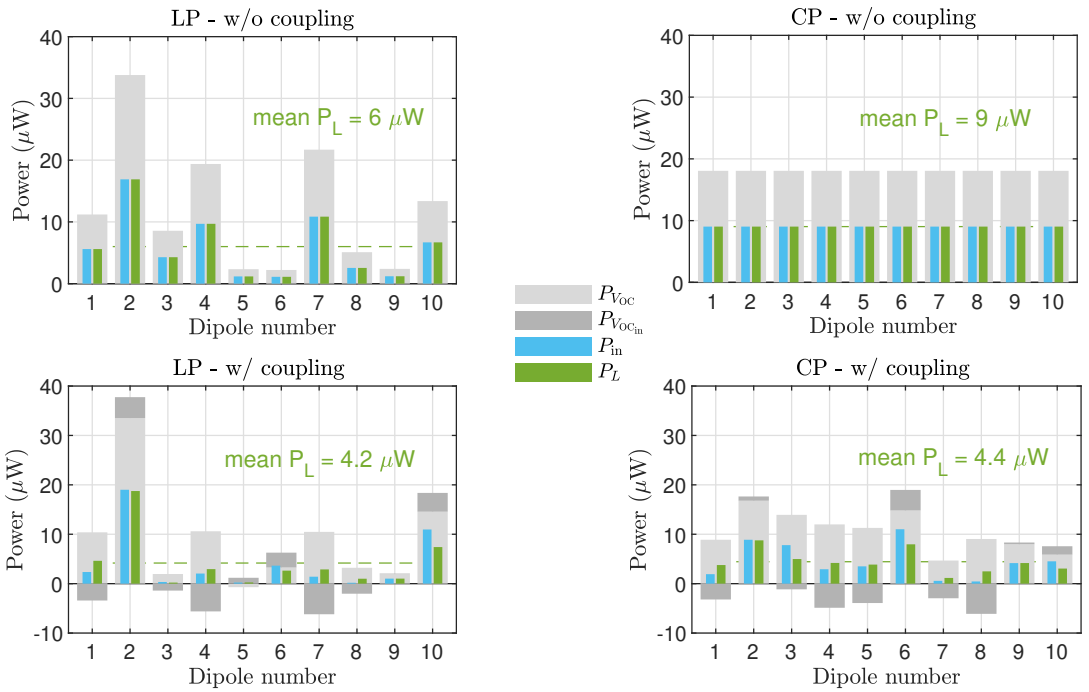

Fig. 11: Power budget for a grid of 10 randomly distributed matched dipoles using linear (LP) and circular (CP) polarisation, with (w/) and without (w/o) mutual coupling.

For both polarisations, the random position and orientation of the dipoles, as well as the coupling between them, result in different power values at the level of the two sources, $P_{V_n^{\mathrm{OC}}}$ and $P_{V_{\mathrm{in}_n}^{\mathrm{OC}}}$. Even though all the dipoles are identical and are connected to their isolated conjugate matched loads, the source power is divided into two unequal parts as a consequence of mismatch due to mutual coupling effects. Consequently, the absorbed (P_{L_n}) and the re-radiated (P_{in_n}) power values are not the same in this case. On average, the absorbed power of the dipoles reduces due to coupling effects. However, the effect of the coupling on each dipole individually is a random phenomenon, e.g. in the case of the linear polarisation, P_{L_2} has slightly increased thanks to the coupling, while P_{L_3} has vanished. Moreover, P_{L_2} decreases with circular polarisation while P_{L_5} increases. The equivalent circuit in Fig. 6(b) shows that the voltage sources have opposite conventions. According to the direction of current flow, a positive power for V_n^{OC} is considered to be supplied while for $V_{\mathrm{in}_n}^{\mathrm{OC}}$ is considered to be received. Consequently, a negative power for $V_{\mathrm{in}_n}^{\mathrm{OC}}$ indicates that the voltage source works as a generator.

The power budget in the presence of coupling shows a significant variability which makes the power prediction for another random distribution of dipoles difficult. The need for a statistical study is also encouraged by comparing the power budget of dipoles with that of T-matched dipoles as well as real tags. In fact, one can normalise the absorbed power by the dipoles, with and without T-match, and the tags distributed as in the configuration shown in Fig. 10 by their respective absorbed powers when they are isolated (Tables II and III). The result is presented in Fig. 12. In Fig. 12(a) and (b), the obtained power values by 4NEC2 are validated by HFSS with a low error. Fig. 12(c) shows that, although the normalised powers for the three antenna types are not identical, there is a clear correlation between the power levels.

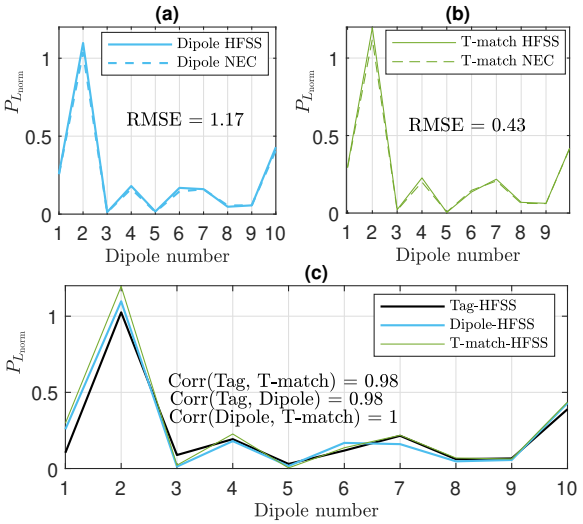

Fig. 12: Normalised absorbed powers ($P_{L_{\mathrm{norm}}}$) of (a) dipoles and (b) T-matched dipoles obtained by NEC and HFSS and (c) compared to those of the tags, in the random configuration shown in Fig. 10 with respect to their respective isolated P_L.

V. Statistical analysis

The deterministic analysis presented in the previous section shows the impact of the randomness and coupling on the power budget of one configuration of dipoles. If different random configurations of the same dipoles with the same density are considered, a statistical analysis becomes mandatory. In this section, we consider 2000 configurations of 10 antennas distributed over two distribution areas of dimensions $1\lambda \times 1\lambda$ and $2\lambda \times 2\lambda$. The statistics of absorbed power P_L is studied for dipoles with and without T-match. As the simulation is much more time-consuming for a tag antenna, the statistical analysis is performed for only one density ($1\lambda \times 1\lambda$) and one polarisation (LP) in the case of real tags. Table IV gives an insight by presenting the mean (μ), the standard deviation (σ), and the coefficient of variation (σ/μ) of the absorbed power for different cases.

TABLE IV: Statistical moments

		μ		σ		σ/μ
		(μW)	(dBm)	(μW)	(dBm)	
				Dipole		
$1\lambda \times 1\lambda$	LP	4.19	-23.78	4.32	-23.65	1.03
	CP	4.19	-23.78	3.02	-25.20	0.72
$2\lambda \times 2\lambda$	LP	7.82	-21.07	6.42	-21.92	0.82
	CP	7.87	-21.04	3.45	-24.62	0.44
				T-match		
$1\lambda \times 1\lambda$	LP	4.96	-23.04	4.88	-23.11	0.98
	CP	4.96	-23.04	3.19	-24.96	0.64
$2\lambda \times 2\lambda$	LP	8.87	-20.56	7.10	-21.49	0.81
	CP	8.85	-20.53	3.58	-24.46	0.40
				Tag		
$1\lambda \times 1\lambda$	LP	3.76	-24.25	3.96	-24.02	1.05

It can be stated that the mean absorbed power is mainly related to the density of dipoles, i.e., the lower the density, the better would be the level of absorbed power. For a given distribution area, the mean power (μ) for the linear and circular polarisations are almost the same. Finally, the dispersion (σ/μ) is always higher for the linear polarisation compared to the circular one.

Valuable information can be extracted from the empirical cumulative distribution functions (CDF) of the normalised power. Fig. 13 presents the CDF for the normalised absorbed power values (20000 samples) when all antennas are terminated with their respective isolated matched loads. According to Table II, with a linearly (vertically) polarised plane wave with $E_Z = 1$ V/m, the power at the load level of an isolated vertical dipole is equal $P_{L_0} = -17.4$ dBm. An isolated dipole inclined at 45° receives half of this power: $P_{L_{45}} = -20.4$ dBm. On the other hand, the mean value of the absorbed power for 20000 dipoles (2000 configurations of 10 dipoles) without coupling is equal to -20.4 dBm. This shows that the 45° inclined dipole can be seen as a good representative of the average polarisation effect in the absence of coupling. According to Table III, with a circularly polarised plane wave with the same field intensity, the power at the load level of

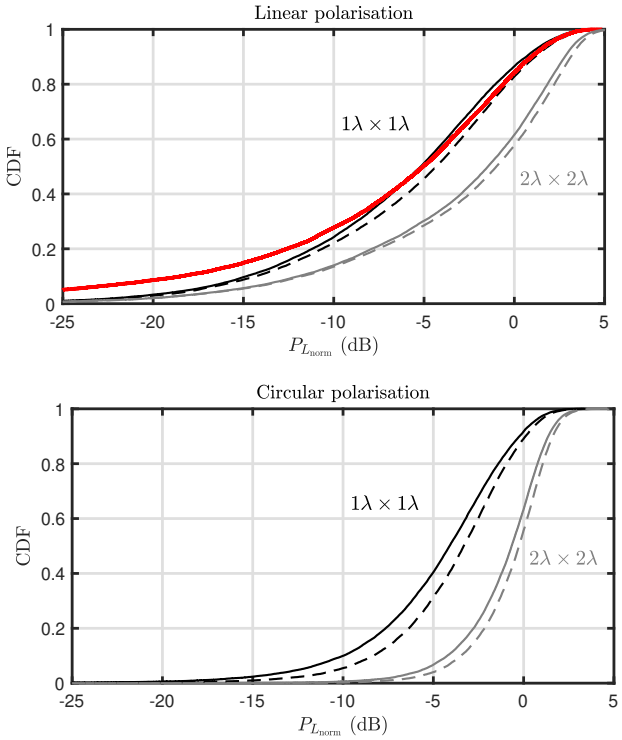

Fig. 13: CDF plots for the normalised absorbed power in 2000 configurations of 10 randomly distributed matched tags (thick red line), dipoles without (solid line) and with (dashed line) T-match, illuminated by linearly and circularly polarised wave over two distribution surface areas.

an isolated vertical dipole is equal to -20.4 dBm, and this would be the absorbed power at the level of any single dipole, regardless of its orientation. The same argument is valid for the dipole with T-match and the tag. Consequently, the CDF plots of Fig. 13 have been traced after normalising the absorbed power in each random configuration by the absorbed power of the antenna illuminated by a circularly polarised plane wave.

We observe that the normalised CDF plots of dipoles with and without T-match are close together, a larger difference appears for the denser configuration. According to this figure, the normalised $P_{L_{\text{norm}}} = 0$ dB represents the absorbed power by the isolated antenna which is called hereafter as $P_{L_{\text{iso}}}$. Let us consider the linear polarisation in the case of $1\lambda \times 1\lambda$ distribution area. By referring to the respective CDF curve in Fig. 13, one may note that 86% of dipoles without T-match and 83% of dipoles with T-match observe a lower power than $P_{L_{\text{iso}}}$ as a result of the mutual coupling. As expected, this percentage is reduced to 62% (without T-match) and 58% (with T-match) for the $2\lambda \times 2\lambda$ randomly distributed case. The same tendency is valid for circular polarisation. The percentage of the dipoles with and without T-match receiving a power lower than the isolated case is approximately equal to 90% for the smaller area and 60% for the larger one.

As for the real tag, the normalised CDF relies close to corresponding CDF plots of Fig. 13. Consequently, the CDF plots can also be used to predict the coupling effects in the case of real tags. Moreover, by adding information about the

tag-to-reader distance involved, the CDF plot can be used to predict the wake-up rate of the tags as well. The normalised power in dB is defined as $P_{L_{\rm norm}} = P_{L_{\rm non-iso}} - P_{L_{\rm iso}}$, where $P_{L_{\rm non-iso}}$ and $P_{L_{\rm iso}}$ are the absorbed powers of the chip in the case of a surrounded tag and an isolated tag, respectively. The normalised power is the same at any distance from the reader. In order to power up a surrounded tag at an arbitrary distance d_0, the chip power in the non-isolated case $P_{L_{\rm non-iso}}$ should be larger than the threshold power of the chip $P_{L_{\rm th}}$. Thus the surrounded tag replies if:

$$P_{L_{\rm non-iso}}\big|_{d=d_0} \geq P_{L_{\rm th}} \tag{11}$$

Subtracting $P_{L_{\rm iso}}|_{d=d_0}$ from both sides of (11):

$$\begin{aligned} P_{L_{\rm non-iso}}\big|_{d=d_0} - P_{L_{\rm iso}}|_{d=d_0} &\geq P_{L_{\rm th}} - P_{L_{\rm iso}}|_{d=d_0} \\ P_{L_{\rm norm}} &\geq P_{L_{\rm th}} - P_{L_{\rm iso}}|_{d=d_0} \end{aligned} \tag{12}$$

In this equation $P_{L_{\rm th}}$ is known by the data-sheet of the chip and $P_{L_{\rm iso}}|_{d=d_0}$ should be estimated or measured for a given tag at distance d_0. The condition obtained in (12) designates the statistics of the replying tags over the normalised CDF curve of Fig. 13. This analysis may lead us to the particular case of the maximum read-range of the system, where $d = d_{\rm max}$ and the absorbed power of an isolated tag is equal to its threshold $P_{L_{\rm iso}}|_{d=d_{\rm max}} = P_{L_{\rm th}}$. Consequently, the condition obtained in (12) is reduced to $P_{L_{\rm norm}} \geq 0$ dB. In this special case, $P_{L_{\rm norm}} \geq 0$ dB over the normalised CDF curve of Fig. 13 designates not only the percentage of tags for which the coupling effects have a beneficial impact, but also those of which are going to be powered up.

VI. Conclusion

In this paper, the degradation in the read-range of an isolated home-made tag has been analysed in the presence of surrounded short-circuited tags on a system-level from measurements and is validated using HFSS simulations. This has led us to extend our work on a circuit-level with a simplified model of an RFID tag surrounded by other loaded tags. We used real commercial UHF RFID tags to analyse the effect of randomness in a high-density context. The observed similarities between the behaviour of the RFID tag and a half-wave dipole allowed a simplification of the tag antenna in order to obtain a low-cost model, where the RFID tags are modelled by a set of half-wave dipoles, with and without T-match, and the reader is replaced by a plane wave. The RFID forward link has been investigated statistically for two different densities of dipoles (with and without T-match) terminated on their matched loads employing linear and circular polarisations, and one density in the case of commercial tags employing linear polarisation. The preliminary statistical results show a non-negligible influence of the coupling on the received power at the level of the chip. This technique allows the quantification of the percentage of tags that are not powered up in a given scenario. Combined with the reverse link, this statistical analysis would help the RFID designer to assess the performance of the RFID link.

VII. Acknowledgments

The authors thank Stéphane Protat and Jimmy Leszczynksi from ESYCOM/UGE for the electromagnetic simulations and the fabrication of the RFID home-made tag.

References

[1] S. A. Ahson and M. Ilyas, *RFID handbook: applications, technology, security, and privacy*. CRC press, 2017.

[2] S. Ebrahimi-Asl, M. T. A. Ghasr, and M. J. Zawodniok, "A solution to low read rate problem in RFID scattering networks," *IEEE Journal of Radio Frequency Identification*, vol. 1, no. 2, pp. 176–184, 2017.

[3] S. Ebrahimi-Asl, M. T. A. Ghasr, and M. Zawodniok, "Cooperative interference control in neighboring passive scattering antennas," *IEEE Journal of Radio Frequency Identification*, vol. 2, no. 3, pp. 152–158, 2018.

[4] J. R. Kruest and G. Bann, "Systems and methods for stirring electromagnetic fields and interrogating stationary RFID tags," U.S. Patent 07, 2011-07-07.

[5] M. Balog, E. Szilagyi, D. Duplakova, and M. Minďaš, "Effect verification of external factor to readability of RFID transponder using least square method," *Measurement*, vol. 94, pp. 233–238, 2016.

[6] J. Bolton, E. Jones, R. K. Punugu, A. Addy, and S. Okate, "Performance and benchmarking of multisurface UHF RFID tags for readability and reliability," *Journal of Sensors*, vol. 2017, 2017.

[7] R. Durgamcherur and E. C. Erick Jones, "Statistical analysis on readability of RFID Gen2 passive tags using bayesian information criterion and 2-level factorial design," *Int. Supply Chain Technol. J.*, vol. 06, no. 11, Nov. 2020.

[8] G. Aryal, L. Mapa, and S. K. Camsarapalli, "Effect of variables and their interactions on RFID tag readability on a conveyor belt—factorial analysis approach," in *2010 IEEE International Conference on Electro/Information Technology*. IEEE, 2010, pp. 1–6.

[9] A. Mughal, S. Mostarshedi, B. Poussot, and J.-M. Laheurte, "Introduction of statistics in the analysis of an RFID link in a high density context," in *2022 IEEE 12th International Conference on RFID Technology and Applications (RFID-TA)*. IEEE, 2022, pp. 224–227.

[10] K. D. Palmer and M. W. van Rooyen, "Simple broadband measurements of balanced loads using a network analyzer," *IEEE transactions on instrumentation and measurement*, vol. 55, no. 1, pp. 266–272, 2006.

[11] *Higgs 9, EPC Class 1 Gen 2 RFID Tag IC*, Alien Technology, 2020. [Online]. Available: https://www.alientechnology.com/products/ic/higgs-9/

[12] L. Catarinucci, D. De Donno, R. Colella, F. Ricciato, and L. Tarricone, "A cost-effective SDR platform for performance characterization of RFID tags," *IEEE Transactions on Instrumentation and Measurement*, vol. 61, no. 4, pp. 903–911, 2011.

[13] P. V. Nikitin, K. V. S. Rao, R. Martinez, and S. F. Lam, "Sensitivity and Impedance measurements of UHF RFID chips," *IEEE Transactions on Microwave Theory and Techniques*, vol. 57, no. 5, pp. 1297–1302, 2009.

[14] I. Adjali, A. Gueye, S. Mostarshedi, B. Poussot, F. Nadal, and J.-M. Laheurte, "Matching evaluation of highly coupled dipoles quantified by a statistical approach," *IEEE Transactions on Antennas and Propagation*, vol. 68, no. 7, pp. 5044–5051, 2020.

[15] J. Mautz and R. Harrington, "Modal Analysis of Loaded N-port Scatterers," *IEEE Transactions on Antennas and Propagation*, vol. 21, no. 2, pp. 188–199, March 1973.

[16] G. Marrocco, "RFID Grids: Part I Electromagnetic Theory," *IEEE Transactions on Antennas and Propagation*, vol. 59, no. 3, pp. 1019–1026, March 2011.

[17] *ALN-9662 Short Inlay*, Alien Technology, 2014. [Online]. Available: http://www.alientechnology.com/wp-content/uploads/Alien-Technology-Higgs-3-ALN-9662-Short.pdf

[18] *Higgs 3, EPC Class 1 Gen 2 RFID Tag IC*, Alien Technology, 2020. [Online]. Available: https://www.alientechnology.com/products/ic/higgs-3

[19] F. Gourari, S. Meriah, S. Protat, J. Dubouil, and J.-M. Laheurte, "Comparison of two matching techniques for UHF RFID tags," *Microwave and Optical Technology Letters*, vol. 60, no. 7, pp. 1763–1767, 2018.

[20] C. A. Balanis, *Antenna Theory: Analysis and Design*. Wiley-Interscience, 2005.

[21] G. J. Burke and A. J. Poggio, "Numerical Electromagnetics Code (NEC)-Method of Moments," *Technical document*, 1981.

Aiman Mughal was born in Pakistan. She received the B.E. degree in telecommunication from MUET in Pakistan in 2015, and the M.Sc. degree from the Université de Bourgogne, Dijon, in 2019. She is currently pursuing the Ph.D. degree with the Laboratoire Electronique, Systèmes de Communication et Microsystèmes (ESYCOM Laboratory), University Gustave Eiffel. Her research interests primarily revolve around electromagnetic theory, with a specific focus on RFID design and RFID chip measurements.

Jithin Mudakkarappilli Sudersanan was born in India. He received the B.Tech. degree in electronics and communication from Mahatma Gandhi University, India, in 2017, and the M.Tech. degree specializing in microwave and radar engineering from the Cochin University of Science and Technology, India, in 2020. He is currently pursuing the Ph.D. degree with the ESYCOM Laboratory, University Gustave Eiffel, France. His research interests revolve around the realms of electromagnetic theory, radio frequency identification technology, and the analysis of tag performance metrics through empirical measurements.

Shermila Mostarshedi received the B.Sc. degree in electrical engineering from Sharif University of Technology, Tehran, Iran, in 1999, the M.Sc. degree in electrical engineering from Tehran Polytechnic in 2003, and the Ph.D. degree from Université Paris-Est Marne-la-Vallée, France, in 2008. She worked as a Telecommunications Engineer with Siemens, Iran, before preparing her Ph.D. degree. She is currently with the Université Gustave Eiffel, where she works as an Associate Professor and is a member of the ESYCOM Laboratory. Her research interests include wave propagation, computational electromagnetics and statistical approaches in electromagnetic problems.

Benoit Poussot received the Ph.D. degree in electronics from Université Paris-Est Marne-la-Vallée in 2007. He was an Electronic Engineer with ESCPI-CNAM in 2004. He is currently an Associate Professor at Université Gustave Eiffel and is a member of ESYCOM Laboratory. He has authored or coauthored more than 40 publications, communications, technical reports, patents and book chapters. His research topics include wave propagation, channel modeling, reconfigurable antenna design, system architecture design for 60 GHz applications, and detection and localisation techniques.

Jean-Marc Laheurte received the M.Sc. and Ph.D. degrees in electrical engineering and the Habilitation à Diriger les Recherches degree from the University of Nice, France, in 1989, 1992, and 1997, respectively. From 1989 to 1990, he was a Research Assistant with the École Polytechnique Fédérale de Lausanne, Switzerland. In 1992, he was a Post-Doctoral Researcher with the University of Michigan, Ann Arbor, MI, USA. From 1993 to 2002, he was an Associate Professor with the University of Nice Sophia Antipolis, France. From 2002 to 2011, he was a Professor with the University Gustave Eiffel, France, where he was the head of the Gaspard Monge Institute for five years. In 2012, he spent one year as an RF Senior Engineer with Tagsys, La Ciotat, France. Since 2014, he is the Director of the Laboratoire Electronique, SYstèmes de COmmunications et Microsystèmes (ESYCOM Laboratory) including 75 members. He has organized several courses in various European institutions in the frame of the European School of Antennas and has been ruling the "Antennas" committee of the French Microwave Conference (JNM) for 10 years. He has authored or co-authored two books, 2 book chapters, over 80 technical papers in international journals, and 100 conference papers. He holds two patents on RFID technologies. His current research interests include antennas in matter, RFID technologies, and wireless monitoring of civil engineering infrastructures.